JACS
JOURNAL OF THE AMERICAN CHEMICAL SOCIETY
pubs.acs.org/JACS

Open Access
This article is licensed under CC-BY 4.0

Article

# Glycosaminoglycans Promote Amyloid-$\beta$ Aggregation via Multivalent, pH-Dependent Interactions

Eunjin Moon, Charlotte Radelof, Jana Sticht, Yu Wang, Felicia Fürstenberg, Clemens Krage, Sebastian Straeten, Wesley Pietsch, Boris Schade, Artem Pavlov, Ricardo Zarate, Gaël M. Vos, Gergo Peter Szekeres, Birgit Strodel, Beate Koksch, Kevin Pagel,* and Nicklas Österlund*

Cite This: J. Am. Chem. Soc. 2026, 148, 49109−49120

Read Online

ACCESS | Metrics & More | Article Recommendations | Supporting Information

**ABSTRACT:** Glycosaminoglycans (GAGs) are polyanionic polysaccharides that colocalize with amyloid deposits in Alzheimer's disease, yet their mechanistic contribution to aggregation remains unclear. Here, we show that GAGs function as pH-responsive electrostatic scaffolds that selectively accelerate A$\beta$(1−42) aggregation under mildly acidic, early endosomal-like conditions but not at neutral pH. Combining experimental and computational approaches, we identify protonated N-terminal histidines as key determinants of GAG binding. Weak interactions between GAGs and the charged N-terminal region of A$\beta$ promote conformational rearrangements that bring peptides into proximity and expose adjacent hydrophobic aggregation-prone segments, thereby facilitating peptide clustering. Kinetic analyses reveal that aggregation is enhanced in a way consistent with an apparent increase in effective peptide concentration, accelerating nucleation without altering the dominant aggregation pathway. Systematic variation of GAG chain length and sulfation level further demonstrates that aggregation enhancement requires a threshold degree of multivalency, consistent with a clustering-driven mechanism. Together, these findings establish a framework in which pH-dependent polyelectrolyte interactions act as molecular triggers of amyloid nucleation and define the physicochemical parameters that govern when GAGs transition from passive interaction partners to active promoters of A$\beta$ aggregation, providing insight into how cellular microenvironments may regulate the earliest stages of Alzheimer's disease pathology.

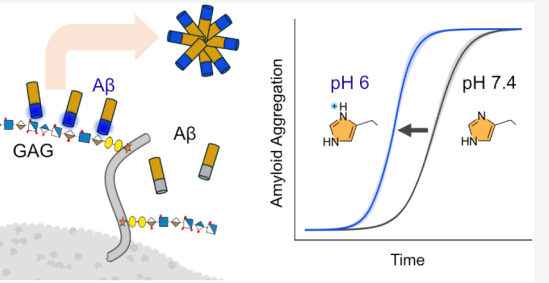


## INTRODUCTION

Glycosaminoglycans (GAGs) are linear anionic polysaccharides that are typically covalently attached to core proteins to form proteoglycans on cell surfaces where they mediate diverse functions, including cell adhesion, signaling, and protein stability and trafficking.[1−3] GAGs are composed of repeating disaccharide units consisting of a hexuronic acid and a hexosamine and are classified into several families, including heparan sulfate/heparin (HS/Hep), chondroitin sulfate and dermatan sulfate (CS/DS), and hyaluronic acid (HA) (Figure 1A).[4] These classes differ in composition and degree of sulfation: HS and Hep are highly sulfated, CS and DS are more moderately sulfated, and HA is unsulfated.[5] The high charge density and structural flexibility of sulfated GAGs enable multivalent interactions with a wide range of proteins, often modulating their conformation and activity.[6−8] Dysregulation of GAG biosynthesis or turnover has been implicated in numerous pathological conditions, including cancer, fibrosis, inflammatory disorders, and neurodegenerative diseases.[6] Notably, GAGs are consistently found as integral components of pathological amyloid deposits in aggregation-related diseases, where they colocalize with and can directly interact with aggregation-prone proteins.[9−13] These pathological interactions may involve either proteoglycans or free GAG chains, such as heparin released during mast cell activation,[14,15] as well as free HS fragments generated locally by endolysosomal heparanase activity.[16,17]

GAGs have been recognized as important modulators of amyloidogenesis across diverse proteins, affecting aggregation rates or inducing specific fibril polymorphs.[13,18,19] In Alzheimer's disease (AD), the amyloid-$\beta$ peptide is known to interact with GAGs, with which they colocalize in senile plaques.[20,21] A$\beta$ peptides are generated through proteolytic processing of the membrane-bound amyloid precursor protein (APP) at the plasma membrane or within endosomes,[22,23] with endosomal cleavage favoring increased A$\beta$ production.[24,25] Among the different A$\beta$ isoforms, the 42-residue-long A$\beta$(1−42) variant is particularly prone to self-assembly into $\beta$-sheet-rich aggregates associated with neurotoxicity.[26] Structurally,

Received: June 24, 2026
Revised: October 5, 2026
Accepted: October 22, 2026
Published: November 5, 2026



ACS Publications
© 2026 The Authors. Published by American Chemical Society



https://doi.org/10.1021/jacs.6c12804
J. Am. Chem. Soc. 2026, 148, 49109−49120

Downloaded from pubs.acs.org/jacsat/article-pdf/148/45/49109/6909223/jacs.6c12804.pdf by FORSCHUNGZENTRUM JUELICH user on 26 November 2026

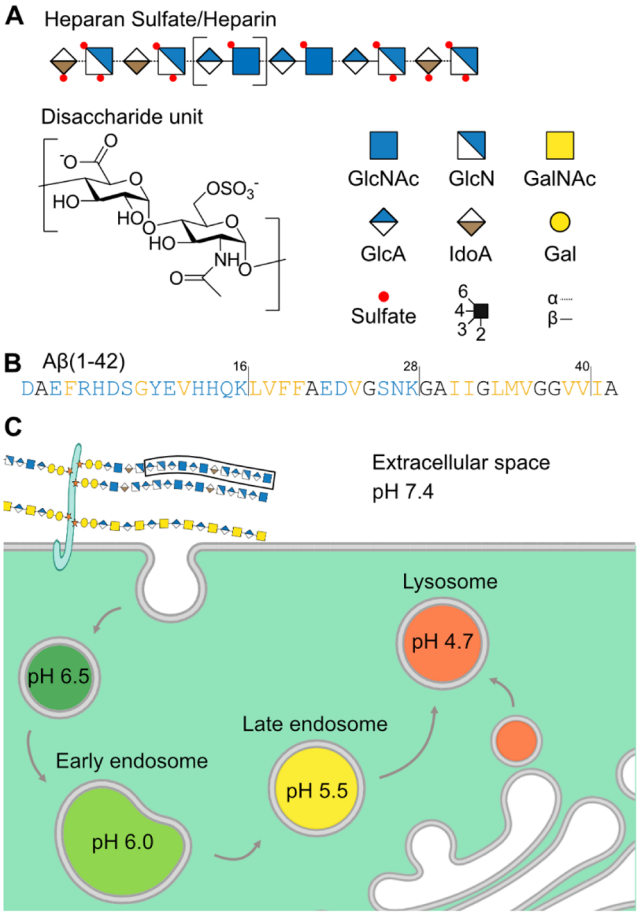


**Figure 1.** GAG and Aβ peptide properties and the pH microenvironments in cellular compartments. A) The GAG disaccharide unit in heparan sulfate is shown as an example along with the SNFG nomenclature for different monosaccharides: *N*-acetylglucosamine (GlcNAc), glucosamine (GlcN), *N*-acetylgalactosamine (GalNAc), glucuronic acid (GlcA), iduronic acid (IdoA), and galactose (Gal). B) The sequence of Aβ(1−42) with hydrophobic residues colored orange and hydrophilic residues colored blue. C) The cartoon depiction of the cellular microenvironments and their respective pH values.

the peptide consists of a hydrophilic N-terminal region, followed by two hydrophobic segments separated by a flexible hinge region (Figure 1B). The aggregation behavior of Aβ is highly sensitive to its microenvironment, including pH,[27] ionic strength,[28] and interactions with biological macromolecules.[29−31]

Importantly, Aβ and GAGs colocalize across distinct cellular compartments with distinct physicochemical properties. At the cell surface, GAGs and proteoglycans facilitate uptake and endocytic trafficking of extracellular Aβ alongside other GAG-binding ligands.[32−35] Upon internalization, these proteoglycan and GAG complexes are directed to early endosomes.[36] This localization is crucial for further trafficking such as recycling of ligands back to the cell surface, sustaining intracellular signaling and degradation.[37] Whereas the extracellular environment is maintained at near-neutral pH, endosomal and lysosomal compartments are increasingly acidic (Figure 1C) and have been proposed as key sites for Aβ aggregation.[38−44] This pH transition is particularly relevant for Aβ because its N-terminal region contains three histidine residues, H6, H13, and H14, whose protonation increases in the endosomal pH range. As protein−GAG interactions are often mediated by clusters of basic residues,[45,46] acidification may convert the N-terminal region of Aβ into a more cationic surface for interaction with anionic GAGs.

While these observations highlight the importance of environmental and molecular factors in peptide−GAG interactions, the underlying mechanisms remain incompletely understood. Previous studies have reported both enhancement and inhibition of Aβ fibril formation in the presence of GAGs.[9,47−49] These findings may arise from inadequate control over multiple key variables, including differences in GAG class, chain length, sulfation pattern, peptide aggregation state, and solution conditions. For example, different GAG classes can exert distinct biological effects, and aberrant heparan sulfate expression has been observed in patients with AD.[50−52] In addition, Aβ may interact differently with GAGs depending on its aggregation state, with stronger binding reported for specific aggregated species.[53,54] These variables make it difficult to distinguish direct effects on soluble Aβ binding from downstream effects on peptide aggregation.

Here, we examine well-defined GAG samples to assess their binding to soluble forms of the Aβ peptide and the effects on aggregation of these peptide species. We first show that GAGs accelerate Aβ(1−42) aggregation selectively at mildly acidic, early endosomal-like, pH and that this behavior is linked to histidine-dependent GAG binding in the N-terminal region. We then map the interaction to two specific N-terminal binding motifs and show how these electrostatic contacts are coupled to peptide−peptide clustering. Finally, we demonstrate that the aggregation-enhancing effect depends on GAG chain length and sulfation, revealing a requirement for multivalent peptide recruitment.

## RESULTS AND DISCUSSION

### Endosomal pH Enables Histidine-Dependent GAG Binding and Accelerates Aggregation

To test whether endosomal acidification activates GAG-mediated Aβ aggregation, we first compared the effect of enoxaparin, a clinically used low-molecular-weight heparin (LMWH), on Aβ(1−42) aggregation at pH 7.4 and pH 6.0. Aggregation was followed by measuring the time-dependent fluorescence of the amyloid-selective probe Thioflavin T (ThT), whose quantum yield increases markedly upon binding to amyloid fibrils.[55] At pH 7.4, Aβ(1−42) alone exhibited an aggregation lag time of 46 ± 1 min, compared with 43 ± 2 min at pH 6.0. Primary nucleation of Aβ is strongly pH-dependent, whereas secondary nucleation is considerably less sensitive to pH.[56] The weak pH dependence observed under our conditions is therefore consistent with a greater contribution from secondary nucleation, in agreement with previous observations.[65] The addition of an equimolar amount of LMWH at pH 7.4 did not alter the ThT fluorescence kinetics compared to the control experiment of Aβ(1−42) alone. In contrast, when the pH was lowered to 6.0, the same amount of LMWH accelerated Aβ aggregation, decreasing the lag time ($t_{lag}$) to 25 ± 0.6 min and increasing the maximum growth rate ($r_{max}$) from 2.45 ± 0.25 $h^{-1}$ to 4.8 ± 0.73 $h^{-1}$ (Figure 2A). Control ThT experiments performed with LMWH in the absence of Aβ confirmed that the GAG component itself does not increase ThT fluorescence (Figure S1). In addition, cryo-EM and CD spectroscopy showed that the increased ThT signal reflected formation of β-sheet-rich fibrillar structures

Downloaded from pubs.acs.org/jacsat/article-pdf/148/45/49109/6090223/jacs.6c12804.pdf by FORSCHUNGZENTRUM JUELICH user on 26 November 2026


https://doi.org/10.1021/jacs.6c12804
J. Am. Chem. Soc. 2026, 148, 49109−49120

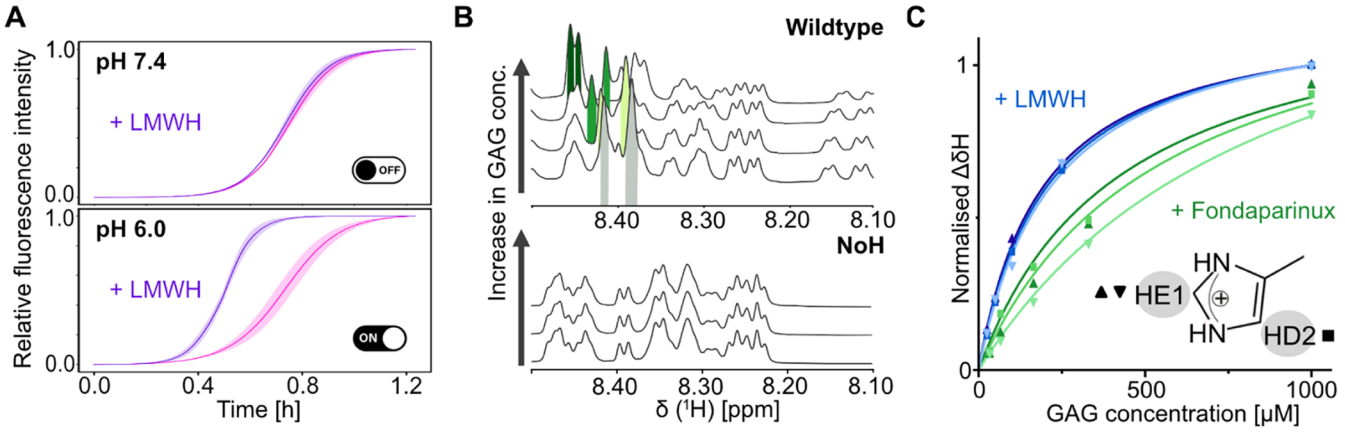


**Figure 2.** Endosomal pH enables histidine-dependent A$\beta$–GAG binding and aggregation. A) Amyloid aggregation of 1 $\mu$M A$\beta$(1–42) followed by monitoring the fluorescence of ThT in the absence (pink) and presence (purple) of low-molecular-weight heparin (LMWH) at pH 7.4 and pH 6.0. B) $^{1}$H NMR spectra of A$\beta$(1–28) and the A$\beta$(1–28) H6A/H13A/H14A triple mutant (NoH) at pH 6.0 upon increasing concentrations of the pentasaccharide fondaparinux. The resonances corresponding to histidine HE1 protons are highlighted. C) Normalized shifts in $^{1}$H chemical shift difference ($\Delta\delta$H) in A$\beta$(1–28) resonances upon titration with LMWH (blue) or fondaparinux (green) at pH 6.0 for HE1 (triangles) and HD2 (squares) resonances.

(Figures S2-3), verifying that the accelerated aggregation observed in the ThT assay still results in amyloid formation, rather than generating more amorphous aggregates, as has been observed in other aggregating systems upon modulating ionic strength[57].

The selective effect of LMWH at pH 6.0 suggested that acidification changes the interaction surface of A$\beta$. Within this pH range, histidines are the main residues expected to undergo substantial changes in protonation. Lowering the pH from 7.4 to 6.0 increases the combined charge of the three histidine residues from +0.36 to +2.32 and shifts the net peptide charge from −2.64 to −0.36 based on experimentally determined p$K_a$ values for A$\beta$ (Figure S4).[58] This effect is concentrated in the N-terminal segment (residues 1–16), which becomes net positively charged at pH 6.0. We therefore asked whether protonated histidines mediate the interaction between A$\beta$ and anionic GAG chains.

To test this interaction mechanism, we synthesized model peptides comprising residues 1–28 of A$\beta$. This segment contains the hydrophilic, pH-sensitive N-terminal region, while removal of the highly hydrophobic C-terminal portion yields a peptide with substantially reduced propensity to aggregate. In this way, we sought to decouple GAG binding from aggregation, enabling an unbiased assessment of the binding mechanism while minimizing interference with peptide aggregation. We synthesized both the wild-type A$\beta$(1–28) sequence and a histidine-substituted variant in which residues H6, H13, and H14 were replaced by alanine (NoH) (Figure S5). Both peptides were C-terminally amidated to avoid introducing a negative charge at position 28, which is not present in the full-length peptide.

Peptide–GAG binding was probed by solution-state $^{1}$H NMR spectroscopy, which allows direct observation of binding without labeling. We first used fondaparinux, a structurally defined heparin pentasaccharide, to reduce the complexity associated with heterogeneous GAG chains. Spectra of the isolated peptide and fondaparinux confirmed that their characteristic resonances did not overlap substantially (Figure S6), and the histidine HE1 and HD2 resonances were assigned using 2D TOCSY and $^{1}$H–$^{13}$C HMQC spectra (Figure S7). Stepwise addition of fondaparinux to wild-type A$\beta$(1–28) caused selective, concentration-dependent chemical-shift changes in histidine resonances (Figure 2B, top). The gradual, concentration-dependent chemical-shift changes are consistent with fast exchange on the NMR time scale, with peak positions reflecting population-weighted averages of the resonance positions of the bound and unbound states, respectively.[59] In contrast, titration of fondaparinux to the NoH control peptide resulted in no detectable spectral changes (Figure 2B, bottom), confirming that histidine residues are essential for GAG binding.

The interaction was also observed with LMWH. Binding curves derived from the affected resonances yielded apparent dissociation constants ($K_d$) of 170 ± 40 $\mu$M for LMWH and 940 ± 270 $\mu$M for fondaparinux, indicating stronger binding to LMWH than to the defined pentasaccharide (Figure 2C). GAG binding at acidic pH was independently confirmed by surface plasmon resonance (SPR) using immobilized LMWH (Figure S8). Upon addition of LMWH, we observed a gradual loss of NMR signal intensity, suggesting that even the low-aggregation-propensity A$\beta$(1–28) peptide may aggregate upon GAG interaction (Figure S9). This effect was much weaker in titrations with fondaparinux. CD spectroscopy confirmed that LMWH induced structural conversion of A$\beta$(1–28) toward $\beta$-sheet, whereas the NoH variant remained largely disordered over the same time course (Figure S10). $\beta$-sheet formation also did not occur at pH 7.4, nor at pH 6 without the addition of LMWH (Figure S11), in accordance with earlier results.[60]

Together, these data establish that mildly acidic pH enables histidine-dependent binding of A$\beta$ to GAGs and that this interaction is sufficient to promote structural conversion toward $\beta$-sheet-rich assemblies. Having established the importance of histidines, we next sought to define the residue-level binding interface and determine how GAG binding is spatially coupled to peptide–peptide interactions.

## GAG Binding Maps to Two N-Terminal Motifs Adjacent to an Aggregation-Prone Segment

To identify the GAG-binding site within A$\beta$, we next performed natural-abundance $^{1}$H–$^{15}$N HSQC experiments. This experiment provides one cross-peak for each backbone amide, generating a 2D fingerprint spectrum in which individual amino acids are better resolved compared to a

Downloaded from pubs.acs.org/jacsat/article-pdf/148/45/49109/6909223/jacs.6c12804.pdf by FORSCHUNGZENTRUM JUELICH user on 26 November 2026


https://doi.org/10.1021/jacs.6c12804
J. Am. Chem. Soc. 2026, 148, 49109–49120

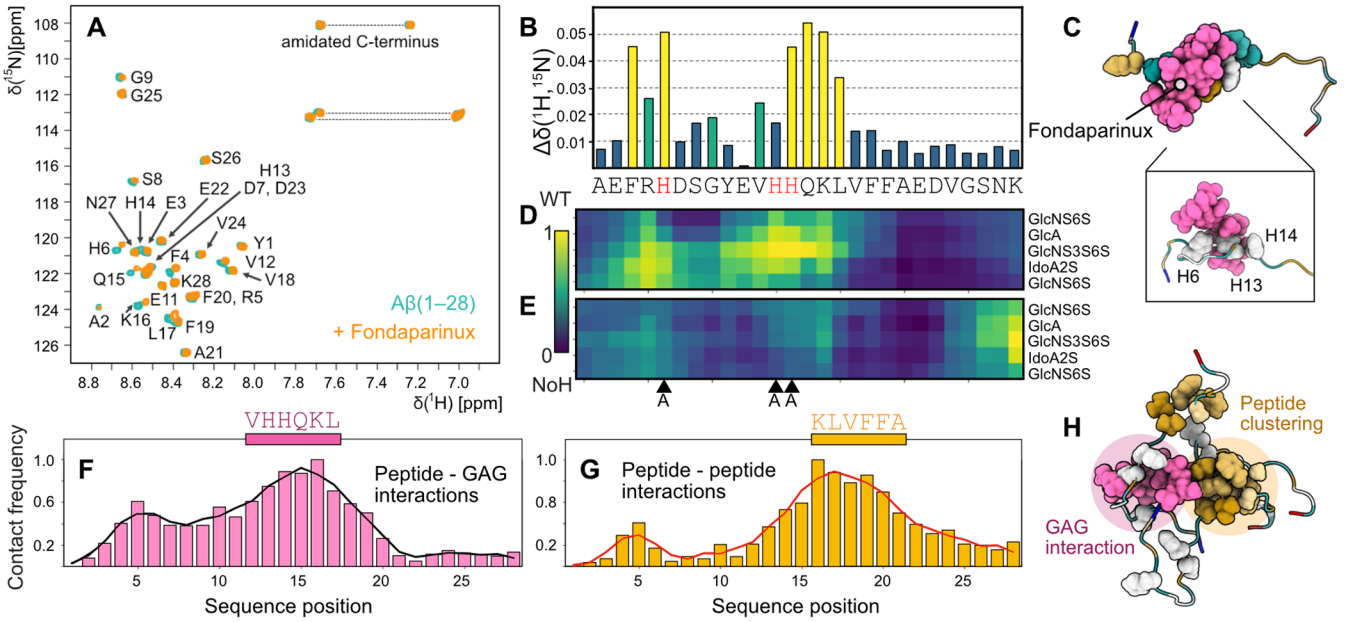


**Figure 3.** Probing the GAG/A$\beta$ binding site. A) $^{1}$H−$^{15}$N HSQC NMR spectra of A$\beta$(1−28) at pH 6.0 before (green) and after (orange) addition of the pentasaccharide fondaparinux. B) Combined chemical-shift perturbation from panel A plotted over the sequence of A$\beta$(1−28). Note that residue D1 is not detected. The major shifts (>mean shift + standard deviation) are colored yellow and minor shifts (>mean shift + half of the standard deviation) green. C) Visualization of the top cluster structure of A$\beta$(1−28) (colored according to hydrophobicity with brown representing hydrophobic residues and blue representing hydrophilic residues) and fondaparinux (pink). The inset shows the interaction between the GAG (pink) and the three histidines of A$\beta$ (gray, spherical representation). D−E) Contact map of the peptide−GAG interactions from MD simulations of the A$\beta$(1−28) (D) and NoH (E) monomers in the presence of one fondaparinux unit. F−G) Relative intermolecular contact frequency between A$\beta$ and fondaparinux (F) and across A$\beta$ peptides (G) in the system comprising three peptides and one GAG molecule. The line represents the running average. H) Visualization of the top cluster structure of three A$\beta$(1−28) peptides (colored according to hydrophobicity) and one fondaparinux molecule (pink). The histidines of A$\beta$ and the central hydrophobic cluster KLVFFA are shown in spherical representation to highlight the distinct peptide−GAG and peptide−peptide interaction hotspots.

one-dimensional $^{1}$H spectrum and can be monitored separately. A$\beta$(1−28) yielded a well-resolved HSQC spectrum (Figure 3A), with cross peaks assigned based on 2D-NOESY, 2D-TOCSY, $^{1}$H−$^{13}$C-HMQC, and $^{1}$H−$^{15}$N-HSQC spectra (Figure S7), also taking into account previously published assignments and predicted chemical shifts (*see Methods in* Supporting Information).[61] Upon titration of fondaparinux, several peptide resonances exhibited clear chemical-shift perturbations. Quantification of these changes using the combined chemical-shift perturbation metric ($\Delta\delta(^{1}H, ^{15}N)$) revealed two distinct regions affected by GAG addition: residues 4−6 and residues 12−17 (Figure 3B). These two clusters include the majority of positively charged residues in the peptide, including $_{12}$VHHQKL$_{17}$, which at low pH conforms to the previously suggested heparin-binding motif XBBXBX, where B is a positively charged residue, and X is any other residue. Notably, the basic residue K28, located in the C-terminal region, did not exhibit detectable perturbations upon GAG addition.

To further elucidate the structural basis of the peptide−GAG interaction, we next turned to molecular dynamics (MD) simulations. All-atom MD simulations were performed in triplicate for A$\beta$(1−28) and NoH monomers with and without fondaparinux at a 1:1 molar ratio. The MD simulations reveal a common binding mode in which the GAG orients approximately perpendicular to the peptide's N-terminal region (Figure 3C). In this arrangement, the central core of the pentasaccharide forms a binding pocket that accommodates the histidine residues of A$\beta$. Analysis of the conformational ensemble indicates that both the wild-type and NoH variants predominantly populate disordered states. However, the wild-type peptide shows a clear propensity for transient $\beta$-hairpin formation, whereas the mutant instead favors $\alpha$-helical conformations, consistent with the helix-stabilizing effect of the alanine substitution. Upon GAG binding, the wild-type peptide adopts a more extended conformation, reflected by an increased N−C terminal distance, a rearrangement associated with facilitating subsequent interpeptide $\beta$-sheet assembly (Figure S12). In contrast, the triple mutant peptide exhibits only minor structural perturbations following GAG addition, with infrequent peptide−GAG contacts and a largely unchanged conformational ensemble (Figure S13).

Consistent with the binding mode identified above, peptide−GAG contact maps of wild-type A$\beta$(1−28) in complex with fondaparinux reveal extensive interactions, indicating near-continuous association between the peptide and the ligand (Figure 3D and S14A). In excellent agreement with the HSQC experiments, two regions showed strong engagement: residues 4−6 around R5, which displayed similar contact probabilities with nearly all monosaccharide rings of the pentasaccharide, and the central segment comprising residues 10−17, which preferentially interacts with the central sugar ring of the GAG pentasaccharide. These interactions are completely absent in the contact map of the NoH variant with fondaparinux (Figure 3E). The total contact frequency of NoH with fondaparinux is only 5% of the contact frequency of the wild-type A$\beta$(1−28), indicating that the remaining positively charged residues are not enough to rescue the interaction (Figure S14B). The highest interactions were confined to K28 and its immediate neighbors (15% contact frequency relative


https://doi.org/10.1021/jacs.6c12804
J. Am. Chem. Soc. 2026, 148, 49109−49120

Downloaded from pubs.acs.org/jacsat/article-pdf/148/45/49109/6909223/jacs.6c12804.pdf by FORSCHUNGZENTRUM JUELICH user on 26 November 2026

to the wild type), whereas R5 and K16 exhibited very low contact probabilities.

To assess the effect of GAG binding on a system of multiple assembling A$\beta$ peptides, we next performed MD simulations of three wild-type A$\beta$(1−28) peptides in the presence of a single fondaparinux molecule. The simulations show that the segment $_{12}$VHHQKL$_{17}$ remains the principal interaction site for fondaparinux in this system as well (Figure 3F). Notably, one peptide acts as the dominant binding partner for fondaparinux, whereas the remaining peptides engage in more diffuse and transient interactions (Figure S15). This behavior is consistent with the preferred GAG interaction site, the central sugar unit of the pentasaccharide, being occupied and thereby limiting equivalent binding by the other peptides. Analysis of intermolecular peptide−peptide contacts reveals a clear preferred interaction hotspot formed by the central hydrophobic cluster $_{16}$KLVFFA$_{21}$, a region well-known for its critical role in A$\beta$ aggregation, which engages in self-association between peptides (Figure 3G, Figure S16).[62] The same aggregation hotspot was also observed in control simulations without GAG (Figure S16), indicating that fondaparinux does not create a new peptide−peptide interface. Instead, GAG binding appears to recruit peptides through the N-terminal histidine-rich region while leaving the intrinsic KLVFFA-mediated self-association interface available for peptide clustering.

To experimentally probe the structural interplay between GAG binding and aggregation, we next analyzed the truncated variants A$\beta$(1−16) and A$\beta$(12−28) in the presence of LMWH using NMR. The N-terminal A$\beta$(1−16) fragment, which lacks the hydrophobic, aggregation-prone region, exhibited histidine-dependent fast-exchange binding behavior similar to that of A$\beta$(1−28), but with reduced line broadening, consistent with diminished aggregation (Figure S17). In contrast, A$\beta$(12−28), which retains the second histidine-rich GAG binding region and the hydrophobic segment, displayed extensive line broadening across the spectrum, indicative of intermediate exchange and/or aggregation (Figure S18). Notably, residues distal to the putative GAG binding site were also affected, suggesting that the observed spectral changes in the spectrum for the 12−28 fragment are dominated by aggregation rather than simple binding.

These observations support the idea that histidine-mediated GAG binding and hydrophobic clustering of peptides are intrinsically coupled processes. The N-terminal region binds to GAGs electrostatically, while the adjacent hydrophobic segment promotes peptide−peptide interactions that compete with or mask GAG binding, leading to apparent changes in exchange behavior and affinity as observed by NMR. The peptide−peptide interaction hotspot is positioned immediately after the peptide−GAG binding region (Figure 3H), suggesting that GAG association promotes spatial clustering of peptides around the GAG scaffold while simultaneously exposing aggregation-prone segments in its vicinity. This arrangement, which affects both local peptide concentration and peptide conformations, is likely to increase the probability of productive nucleation events during assembly.

## GAGs Increase the Apparent A$\beta$ Concentration during Aggregation

To test the idea that the polyanionic GAG chain changes the concentration dependence of aggregation by promoting peptide clustering, we next conducted ThT kinetic experiments at varying A$\beta$ monomer concentrations ($m_0$) with and without LMWH (Figure 4A−B). It is well established that the aggregation half-time ($t_{1/2}$), which scales proportionally with $t_{lag}$, exhibits a power-law dependence on $m_0$ according to $t_{1/2}$ = A $m_0^{\gamma}$, where $\gamma$ is the apparent reaction order of the aggregation process, and A is a kinetic prefactor.[63−65] For aggregation dominated by secondary nucleation, $\gamma$ is given by $\gamma = -(n_2+1)/2$, where $n_2$ is the critical nucleus size for secondary nucleation. For A$\beta$(1−42) at pH 8, $\gamma$ values between −1.5 and −1 have been reported.[66,67] In our data at pH 6, we observe $\gamma$ = −0.47 ± 0.04 for 0.5−3 $\mu$M A$\beta$(1−42) (Figure 4C). This value, close to $\gamma$ = −1/2, indicates saturation of the secondary

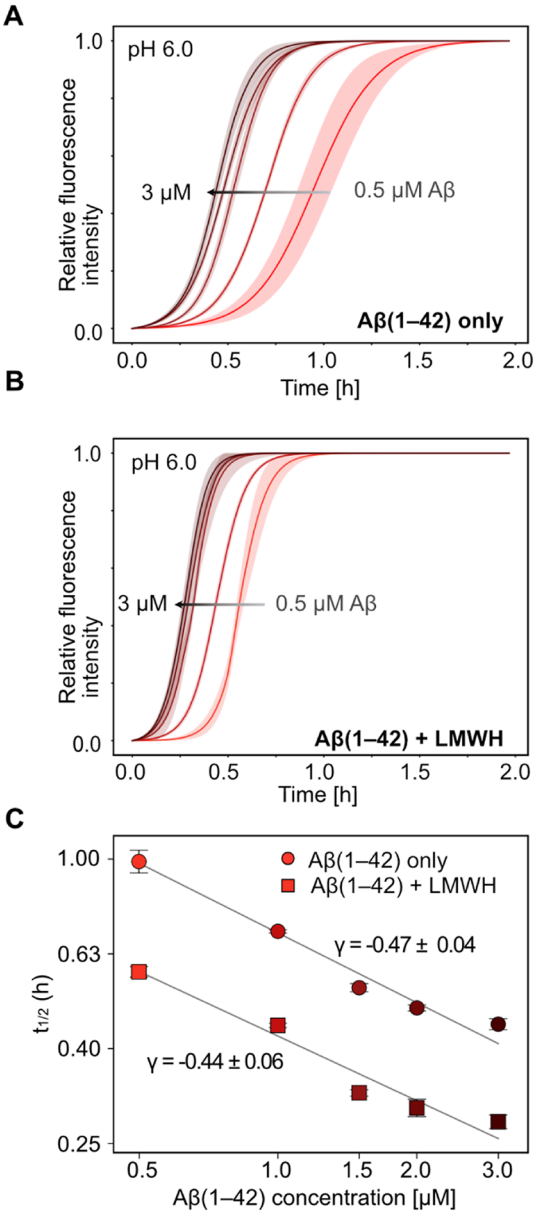


**Figure 4.** The effect of LMWH on the concentration dependence of amyloid aggregation kinetics. A−B) Amyloid formation kinetics at 0.5−3 $\mu$M of A$\beta$(1−42) in the absence (A) and presence (B) of LMWH at pH 6.0. C) Aggregation half-times ($t_{1/2}$) extracted from panels A and B, plotted against monomer A$\beta$(1−42) concentration ($m_0$) in a log−log representation. The data series are fitted to a power law $t_{1/2}$ = A $m_0^{\gamma}$.



https://doi.org/10.1021/jacs.6c12804
J. Am. Chem. Soc. 2026, 148, 49109−49120

Downloaded from pubs.acs.org/jacsat/article-pdf/148/45/49109/6909223/jacs.6c12804.pdf by FORSCHUNGZENTRUM JUELICH user on 26 November 2026

nucleation step ($n_2$ = 0) within this peptide concentration range. In this regime, nucleation occurs when the fibril surface is fully occupied. At lower pH, closer to the isoelectric point of the peptide (pI = 5.4), saturation is likely promoted by reduced electrostatic repulsion and more favorable adsorption to the fibril surface compared to pH 8.[27,66]

Addition of LMWH does not significantly alter $\gamma$, indicating that the dominant aggregation mechanism remains unchanged. However, the absolute rates are systematically increased, as evidenced by a uniform shift of $t_{1/2}$ toward lower values across all A$\beta$ concentrations (Figure 4C). This acceleration is accompanied by a corresponding increase in the maximum aggregation rate $r_{max}$ (Figure S19), consistent with the expected interdependence of $t_{1/2}$ and $r_{max}$ for aggregation dominated by secondary nucleation.[68] Data obtained in the absence and presence of LMWH cluster separately but fall along the same trend line (Figure S20), further supporting a common underlying aggregation mechanism with and without LMWH. The parallel shift in the concentration-dependence plot can be described operationally as an increase in the apparent A$\beta$ concentration in the presence of LMWH. Based on this shift, the effective concentration of A$\beta$ in the LMWH-containing samples is approximately 3-fold higher than in the GAG-free control (Figure S21). Mathematically, the same shift could also arise from a decrease in the kinetic prefactor $A$, corresponding to an increase in one or more microscopic rate constants. Such an effect could result from GAG-induced changes in peptide conformational sampling, as is also suggested by the MD simulations. The ensemble kinetics therefore most likely reflect a combination of scaffold-driven peptide enrichment and increased sampling of nucleation-competent conformations. However, both interpretations are consistent with a model in which GAGs promote aggregation by bringing A$\beta$ molecules into a more aggregation-prone local environment. This model makes a direct prediction: the aggregation-enhancing effect should depend on the ability of the GAG chain to support multivalent peptide recruitment, and therefore on chain length and charge density rather than simply on the total amount of charged carbohydrate present.

## Aggregation Enhancement Requires Multivalent GAG Scaffolding

To investigate the effect of GAG chain properties systematically, we applied multidimensional separation to fractionate LMWH into well-defined populations based on size and net charge. Size-exclusion chromatography (SEC) first resolved the sample into GAG chains spanning 4 to 16 monosaccharide units (dp4−dp16) (Figure 5A). The fractions could be reliably assigned up to dp14, whereas the next fraction likely contains a mixture of longer chains ≥ dp16. Equimolar amounts of the isolated GAG fractions were then incubated together with A$\beta$(1−42) and analyzed by the ThT aggregation assay. A clear dependence on GAG chain length was observed, with progressively stronger acceleration of aggregation for longer chain lengths (Figure 5B). A systematic increase in aggregation rate was evident as polymer length increased, yielding an approximately 40% reduction in the aggregation halftime between dp4 and dp16 (Figure S22A). Consistently, $r_{max}$ increased steeply as GAG length increased (Figure S22B). For both parameters, an apparent saturation of the effect could be observed for the longest chain lengths.

It could be argued that incubating A$\beta$ with equimolar concentrations of GAG chains of increasing length results in a higher total number of monosaccharide units in samples containing longer chains. To distinguish between an effect arising from total GAG content and one intrinsic to chain length, we next compared the fractionated LMWH dp4 and dp8 fractions, as well as the free HS disaccharide (dp2, the smallest unit in a GAG), while varying the total disaccharide unit concentration for each chain length between 1 and 10 $\mu$M.

At matched disaccharide-unit concentrations, dp2 and dp4 showed only weak effects on aggregation, with minimal

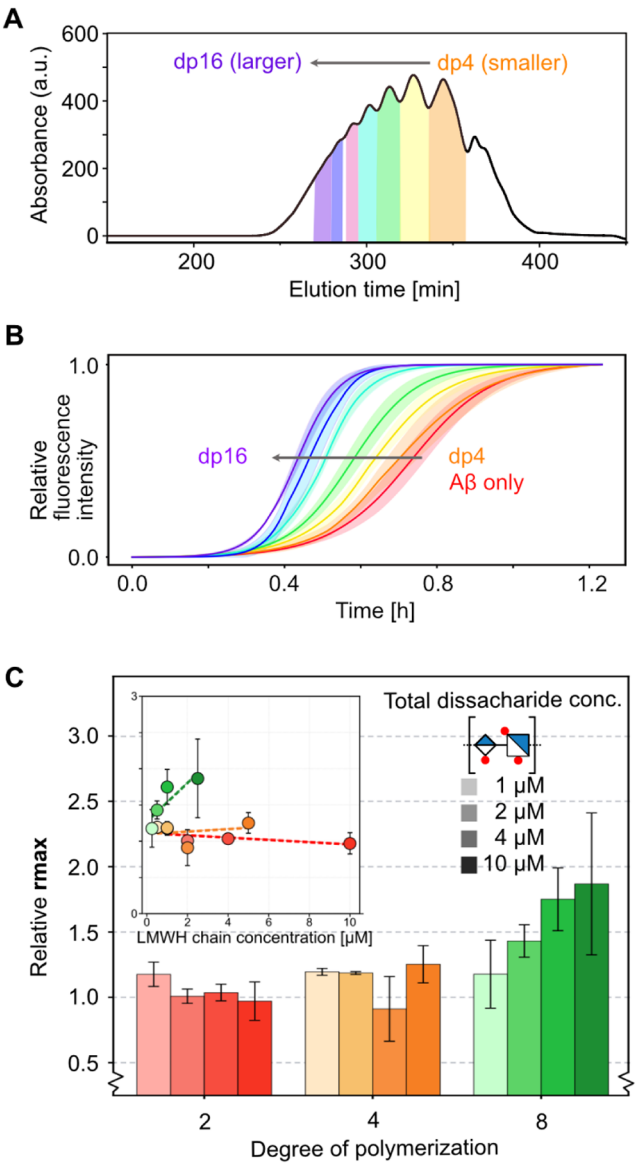


**Figure 5.** The effect of GAG chain length on A$\beta$ aggregation. A) Size fractionation of LMWH by size exclusion chromatography into fractions of distinct chain length (degree of polymerization, dp), indicated by the colors: dp4 (orange), dp6 (yellow), dp8 (green), dp10 (light blue), dp12 (pink), dp14 (dark blue), and ≥dp16 (purple). B) ThT aggregation kinetics of 1 $\mu$M A$\beta$(1−42) at pH 6.0, without addition of heparin (red) and after equimolar additions of distinct chain lengths of LMWH (orange−purple) according to the fractionation in panel A. C) Relative $r_{max}$ comparison from different dp of HS and LMWH (HS dp2, LMWH dp4, and dp8) upon increase of the total disaccharide unit concentration (1−10 $\mu$M). The inset shows the corresponding $r_{max}$ as a function of chain concentration, with the chain concentration being the disaccharide concentration/(degree of polymerization/2).

Downloaded from pubs.acs.org/jacsat/article-pdf/148/45/49109/6909223/jacs.6c12804.pdf by FORSCHUNGZENTRUM JUELICH user on 26 November 2026



https://doi.org/10.1021/jacs.6c12804
J. Am. Chem. Soc. 2026, 148, 49109−49120

changes across the tested concentration range (Figure 5C, red and orange). In contrast, dp8 exhibited a clear concentration-dependent enhancement of aggregation (Figure 5C, green). This effect occurs despite dp8 being present at lower molar chain concentrations compared to dp2 and dp4 at equivalent disaccharide levels (Figure 5C, inset). For example, 2.5 $\mu$M dp8 (equivalent to 10 $\mu$M disaccharide units) produced an approximately 2-fold increase in aggregation rate, whereas 10 $\mu$M of the free disaccharides (dp2) showed no significant effects. These findings suggest that the major contribution to the enhancing effect on aggregation arises from chain-length-dependent multivalency rather than the total number of charged sugar units in solution, thereby arguing against a simple ionic-strength effect. Instead, they indicate that a minimum GAG chain length is required for efficient promotion of aggregation, consistent with a threshold for multivalent peptide recruitment.

Having established that aggregation enhancement depends on chain-length-dependent multivalency, we next considered how the strength of these interactions is influenced by GAG charge density. While longer chains provide a higher total negative charge, effective peptide accommodation could rely on cooperative contributions from chain length and charge distribution, rather than on a single driving factor. To disentangle these contributions, we specifically examined the role of sulfation, which modulates the local charge density along the polymer and thus represents an additional key parameter governing GAG−protein interactions. To examine this, the LMWH dp12 fraction isolated by SEC was further fractionated by anion-exchange chromatography (AXC). AXC of dp12 yielded multiple peaks separated according to net charge (Figure 6A). In comparison, AXC fractionation of dp4 resulted in a chromatogram shifted toward lower elution volumes, consistent with a lower net charge, and displayed a narrower distribution (Figure S23), reflecting the more limited number of possible sulfation patterns in shorter chains. For dp12, the most abundant species (Figure 6A, blue) and a more highly charged fraction (Figure 6A, purple) were isolated, and their effects on A$\beta$ aggregation were assessed using the ThT assay. The results show that the more highly sulfated dp12 heparin accelerates aggregation more strongly, as evidenced by shorter $t_{1/2}$ and an increased $r_{max}$ compared to the lower-sulfated fraction (Figure 6B, Figure S24), highlighting the importance of GAG charge, at a fixed chain length, in promoting amyloid formation.

Since other naturally occurring GAG classes generally exhibit lower degrees of sulfation than heparin, we next compared how different GAG types affect A$\beta$ aggregation. Unsulfated hyaluronic acid (HA), as well as the more weakly sulfated chondroitin sulfate A (CSA) and dermatan sulfate (DS), were evaluated alongside highly sulfated heparin. All GAGs were size-fractionated by SEC, and dp12 fractions were used for the aggregation assays to ensure comparable chain length. A consistent trend was observed in which non- or weakly sulfated GAGs induced only modest reductions in $t_{1/2}$ relative to A$\beta$ alone, whereas highly sulfated heparin produced a substantially stronger acceleration of aggregation (Figure S24). Because these GAG classes differ not only in sulfation level but also in backbone composition, conformation, and sulfate presentation, the stronger effect of heparin likely reflects both higher charge density and favorable spatial presentation of anionic groups.

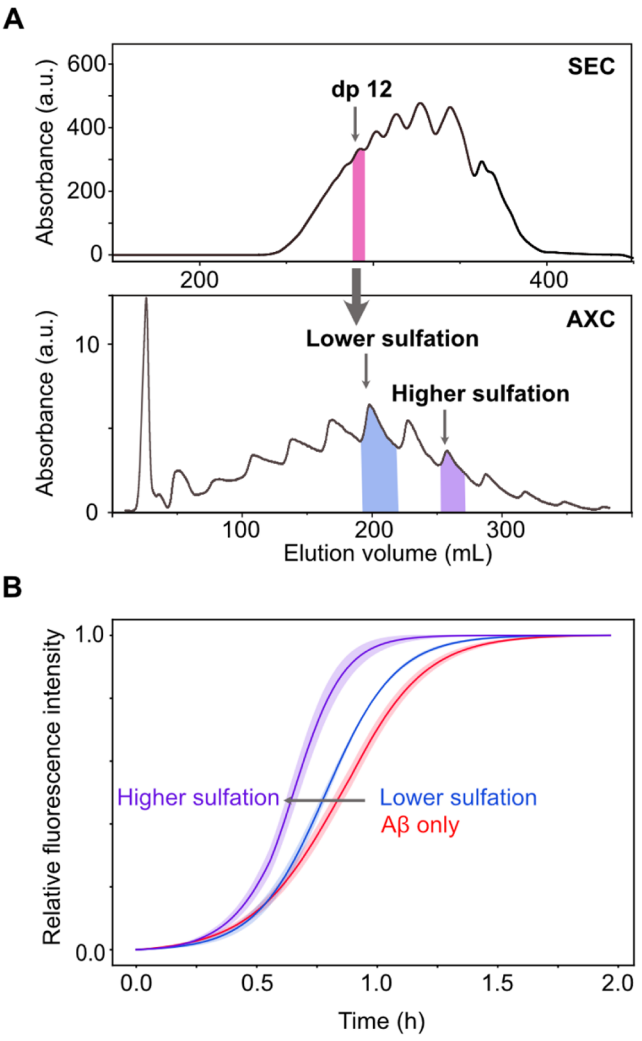


**Figure 6.** Effects of GAG sulfation on A$\beta$ aggregation. A) Multidimensional separation of LMWH, first by size-exclusion chromatography (SEC) followed by anion-exchange chromatography (AXC) of the dp12 fraction from SEC into fractions of distinct degrees of sulfation. B) ThT assay of 1 $\mu$M A$\beta$(1−42) together with equimolar concentrations of dp12 heparin fractions with higher (purple) and lower (blue) degrees of sulfation.

Together, these results demonstrate that GAG-mediated aggregation enhancement is governed by charge-dependent, multivalent interactions, with longer chains and higher sulfation promoting stronger effects by more efficiently clustering A$\beta$ around the GAG scaffold.

## Concluding Remarks

We have shown here that GAGs are pH-dependent modulators of A$\beta$ aggregation kinetics, without substantially altering the dominant aggregation mechanism or diverting aggregation away from $\beta$-sheet-rich amyloid fibril formation. Our results establish a mechanistic framework in which weak multivalent electrostatic interactions between GAGs and the pH-sensitive A$\beta$ N-terminus promote peptide clustering facilitated by the hydrophobic C-terminal segment of the peptide. Such a switchable aggregation behavior provides an interesting mechanism for how the cell could be stressed during disease-related conditions, possibly triggering or enhancing the amyloid cascade observed in AD.

Downloaded from pubs.acs.org/jacsat/article-pdf/148/45/49109/6909623/jacs.6c12804.pdf by FORSCHUNGZENTRUM JUELICH user on 26 November 2026



https://doi.org/10.1021/jacs.6c12804
J. Am. Chem. Soc. 2026, 148, 49109−49120

This pH dependence is particularly relevant in the cellular environments in which Aβ and GAGs encounter one another. While both components are widely present in biological systems, productive aggregation is likely to depend on local microenvironmental changes. Altered GAG composition, including increased accumulation of heparan sulfate proteoglycans and changes in sulfation patterns, has been associated with AD.[52,69] In addition, altered trafficking of GAGs or Aβ may further contribute to this process,[32,70] as Aβ is processed through endosomal−lysosomal pathways and disruptions in these trafficking routes are known to promote its accumulation and aggregation.[34,71] Local acidification may further enhance this effect. Decreased pH in brain tissue and cerebrospinal fluid has been reported in AD,[72] potentially reflecting metabolic dysfunction and elevated lactate levels associated with a shift toward glycolytic metabolism.[73] Activated microglia surrounding plaques may also contribute to localized extracellular acidification through inflammatory and metabolic activity.[74−76] Our results suggest that such changes in pH could directly regulate Aβ−GAG interactions by switching the N-terminal region of Aβ into a more GAG-binding-competent state.

A central finding is the role of histidine protonation as a molecular switch that modulates electrostatic interactions with negatively charged sulfate groups on GAGs. Across GAGs with varying degrees of sulfation, our data indicate that sulfation strongly enhances GAG-mediated aggregation and likely strengthens binding, supporting a charge-driven interaction mechanism. These interactions occur via defined N-terminal motifs that resemble canonical heparin-binding sequences and are positioned directly adjacent to the central hydrophobic cluster (KLVFFA) in Aβ. This spatial proximity between the proposed GAG−recognition site and the aggregation hotspot likely facilitates coupling between GAG binding and peptide−peptide interactions. Importantly, our data show that GAGs do not fundamentally change the aggregation mechanism but instead increase the underlying rates. The net positive charge of the Aβ N-terminal segment and the net negative charge of the GAG chain arguably allow the GAGs to act as dynamic scaffolds that transiently concentrate multiple peptides within a confined volume, consistent with the apparent increase in effective peptide concentration. Such an aggregation environment would be important *in vivo,* where the available Aβ concentration is much lower than the concentrations needed for spontaneous amyloid formation in simple *in vitro* systems.[77] It should be noted that the current study used free GAGs, whereas in biological systems, GAGs are also presented as proteoglycans at membrane surfaces. Membrane-anchored GAGs may further enhance local peptide concentration and further confine the interaction environments. In addition, membrane environments could upshift the $pK_a$ of histidine residues, making protonation and hence peptide−GAG interactions yet more favorable.[58]

The dependence on GAG chain length and sulfation density further supports the proposed model. Short or weakly sulfated GAGs bind peptides but do not efficiently promote aggregation, whereas longer, highly sulfated chains enable multivalent recruitment and cooperative clustering. This distinction indicates that binding alone is not sufficient for aggregation enhancement. Rather, a threshold level of multivalency is required to convert weak peptide−GAG interactions into productive amyloid-promoting scaffolds. The observed GAG binding is weak and occurs at a fast exchange rate on the NMR time scale, corresponding to $\sim 10^3-10^5\ s^{-1}$ (μs−ms time scale).[78] This likely gives rise to a rather "fuzzy" peptide coating of the GAG chain with constant exchange of bound and unbound species. In such a system, aggregation enhancement is not expected to scale simply with binding affinity. Instead, it depends on whether the GAG chain can recruit and spatially organize enough peptide molecules to favor productive peptide−peptide contacts.

Very short GAGs, such as the disaccharide unit (dp2), are too small to facilitate the peptide clustering. Molecular dynamics simulations of fondaparinux, comparable in size to dp4, indicate that this length primarily supports the binding of a single peptide, explaining its limited effect on aggregation compared with longer chains. Such longer GAG chains would, in contrast, enable the simultaneous recruitment of multiple peptides, promoting cooperative assembly. Our data thus suggest a threshold chain length required for efficient aggregation enhancement, consistent with a transition from monovalent to multivalent binding. This observed threshold aligns closely with the intrinsic chain flexibility of the polymer, given that the persistence length of heparin is approximately 2.11 nm (roughly corresponding to dp4),[79] and oligosaccharides shorter than dp6 act as essentially rigid rods, limiting their structural capacity to recruit multiple peptide units. For highly sulfated variants, this persistence length can extend further, reinforcing a rigid conformation that restricts cooperative peptide recruitment at lower degrees of polymerization.[5] Interestingly, the effect of chain length appears to plateau at higher degrees of polymerization, suggesting that beyond a certain length, additional increases in chain size do not enhance clustering. This may reflect a balance between peptide recruitment and spatial dispersion along the polymer, particularly under conditions of a limited peptide availability.

Our results help reconcile previously conflicting reports regarding the role of GAGs in Aβ aggregation.[9,47,48] The present work suggests that GAG activity is highly context-dependent, with pH, multivalency, and GAG sulfation acting as key determinants of whether GAGs act as passive bystanders or active aggregation promoters. More broadly, our findings support a model in which GAGs act as dynamic scaffolds that concentrate and organize aggregation-prone peptides, thereby lowering the energetic barrier to amyloid formation, potentially contributing to the amyloid cascade during disease events. Our study further clarifies the role of the hydrophilic N-terminal segment as a modulating switch during aggregation. Notably, the identified GAG-binding region is not fully conserved across species: rodent Aβ contains substitutions within this segment (R5G, Y10F, H13R) that reduce its positive charge and alter its interaction properties, but does not contain any substitutions within the hydrophobic aggregation-prone regions.[80] It may therefore be speculated that altered GAG binding contributes to the reduced aggregation propensity and amyloid pathology observed in rodents.[81] The GAG-binding motif further overlaps with well-known metal-ion binding sites in the Aβ peptide,[82,83] which are generally considered to slow down amyloid formation, suggesting a possibility of more complex interplay among peptide, GAGs, and other interaction partners.[21,83] Importantly, this also suggests that disrupting electrostatic peptide−GAG interactions, such as through competitive binding to the N-terminal region of Aβ, may provide a strategy to attenuate GAG-triggered aggregation.

Downloaded from pubs.acs.org/jacsat/article-pdf/148/45/49109/6909223/jacs.6c12804.pdf by FORSCHUNGZENTRUM JUELICH user on 26 November 2026



https://doi.org/10.1021/jacs.6c12804
J. Am. Chem. Soc. 2026, 148, 49109−49120

## ■ ASSOCIATED CONTENT

### Supporting Information

The Supporting Information is available free of charge at https://pubs.acs.org/doi/10.1021/jacs.6c12804.

Materials and methods; peptide synthesis and characterization; ThT aggregation, CD, cryo-EM, SPR, NMR, and molecular dynamics supporting data; GAG fractionation and aggregation analyses; Supporting Figures S1−S24 (PDF)

## ■ AUTHOR INFORMATION


### Corresponding Authors

**Kevin Pagel** − *Institute of Chemistry and Biochemistry, Freie Universität Berlin, Berlin 14195, Germany; Research Building SupraFAB, Freie Universität Berlin, Berlin 14195, Germany; Department of Molecular Physics, Fritz Haber Institute of the Max Planck Society, Berlin 14195, Germany;* orcid.org/0000-0001-8054-4718; Email: kevin.pagel@fu-berlin.de

**Nicklas Österlund** − *Institute of Chemistry and Biochemistry, Freie Universität Berlin, Berlin 14195, Germany; Research Building SupraFAB, Freie Universität Berlin, Berlin 14195, Germany; Department of Molecular Physics, Fritz Haber Institute of the Max Planck Society, Berlin 14195, Germany;* orcid.org/0000-0003-0905-7911; Email: nicklas.osterlund@fu-berlin.de

### Authors

**Eunjin Moon** − *Institute of Chemistry and Biochemistry, Freie Universität Berlin, Berlin 14195, Germany; Research Building SupraFAB, Freie Universität Berlin, Berlin 14195, Germany*

**Charlotte Radelof** − *Institute of Chemistry and Biochemistry, Freie Universität Berlin, Berlin 14195, Germany; Research Building SupraFAB, Freie Universität Berlin, Berlin 14195, Germany*

**Jana Sticht** − *Institute of Chemistry and Biochemistry, Freie Universität Berlin, Berlin 14195, Germany*

**Yu Wang** − *Faculty of Mathematics and Natural Sciences, Heinrich Heine University Düsseldorf, Düsseldorf 40225, Germany; Institute of Biological Information Processing: Structural Biochemistry (IBI-7), Forschungszentrum Jülich, Jülich 52428, Germany*

**Felicia Fürstenberg** − *Institute of Chemistry and Biochemistry, Freie Universität Berlin, Berlin 14195, Germany*

**Clemens Krage** − *Institute of Chemistry and Biochemistry, Freie Universität Berlin, Berlin 14195, Germany; Research Building SupraFAB, Freie Universität Berlin, Berlin 14195, Germany*

**Sebastian Straeten** − *Faculty of Mathematics and Natural Sciences, Heinrich Heine University Düsseldorf, Düsseldorf 40225, Germany*

**Wesley Pietsch** − *Institute of Chemistry and Biochemistry, Freie Universität Berlin, Berlin 14195, Germany; Research Building SupraFAB, Freie Universität Berlin, Berlin 14195, Germany*

**Boris Schade** − *Research Center of Electron Microscopy, Freie Universität Berlin, Berlin 14195, Germany*

**Artem Pavlov** − *Institute of Chemistry and Biochemistry, Freie Universität Berlin, Berlin 14195, Germany;* orcid.org/0009-0005-1538-6166

**Ricardo Zarate** − *Institute of Chemistry and Biochemistry, Freie Universität Berlin, Berlin 14195, Germany; Research Building SupraFAB, Freie Universität Berlin, Berlin 14195, Germany*

**Gaël M. Vos** − *Institute of Chemistry and Biochemistry, Freie Universität Berlin, Berlin 14195, Germany; Research Building SupraFAB, Freie Universität Berlin, Berlin 14195, Germany; Department of Molecular Physics, Fritz Haber Institute of the Max Planck Society, Berlin 14195, Germany*

**Gergo Peter Szekeres** − *Institute of Chemistry and Biochemistry, Freie Universität Berlin, Berlin 14195, Germany; Research Building SupraFAB, Freie Universität Berlin, Berlin 14195, Germany; Department of Molecular Physics, Fritz Haber Institute of the Max Planck Society, Berlin 14195, Germany;* orcid.org/0000-0002-4597-6264

**Birgit Strodel** − *Faculty of Mathematics and Natural Sciences, Heinrich Heine University Düsseldorf, Düsseldorf 40225, Germany; Institute of Biological Information Processing: Structural Biochemistry (IBI-7), Forschungszentrum Jülich, Jülich 52428, Germany;* orcid.org/0000-0002-8734-7765

**Beate Koksch** − *Institute of Chemistry and Biochemistry, Freie Universität Berlin, Berlin 14195, Germany; Research Building SupraFAB, Freie Universität Berlin, Berlin 14195, Germany;* orcid.org/0000-0002-9747-0740

Complete contact information is available at: https://pubs.acs.org/10.1021/jacs.6c12804


### Notes

The authors declare no competing financial interest.

## ■ ACKNOWLEDGMENTS

This work was supported by DFG, the German Research Foundation, through GRK2662, grant number 434130070, to EM, CR, CK, BK, and KP. YW and BS gratefully acknowledge computing time on the supercomputer JURECA at Forschungszentrum Jülich under grant AMYAI. YW is supported by a PhD fellowship from the China Scholarship Council. NÖ is supported by a fellowship from the Wenner-Gren Foundations. We acknowledge the research infrastructure and support provided by the SupraFAB Research Facility, funded by the German Federal Government and the State of Berlin. We further acknowledge the assistance of the NMR Core Facility at BioSupraMol, Freie Universität Berlin, supported by the DFG (the German Research Foundation). Dr. Mario Schubert is thanked for the valuable discussion regarding the NMR analysis, and Dr. Allison Ann Berger is thanked for proof-reading the manuscript.

## ■ REFERENCES

(1) Linhardt, R. J.; Toida, T. Role of Glycosaminoglycans in Cellular Communication. *Acc. Chem. Res.* **2004**, *37* (7), 431−438.

(2) Couchman, J. R. Transmembrane Signaling Proteoglycans. *Annu. Rev. Cell Dev. Biol.* **2010**, *26* (26), 89−114.

(3) Basu, A.; Patel, N. G.; Nicholson, E. D.; Weiss, R. J. Spatiotemporal diversity and regulation of glycosaminoglycans in cell homeostasis and human disease. *Am. J. Physiol.: cell Physiol.* **2022**, *322* (5), C849−C864.

(4) Gandhi, N. S.; Mancera, R. L. The structure of glycosaminoglycans and their interactions with proteins. *Chem. Biol. Drug Des.* **2008**, *72* (6), 455−482.

Downloaded from pubs.acs.org/jacsat/article-pdf/148/45/49109/6909223/jacs.6c12804.pdf by FORSCHUNGZENTRUM JUELICH user on 26 November 2026

(5) Szekeres, G. P.; Moon, E.; Elter, J. K.; Roper, B.; Kizhakkedathu, J. N. N.; Ballauff, M.; Haag, R.; Pagel, K. Glycosaminoglycans as Polyelectrolytes: Charge, Interactions, and Applications. *ChemBiochem.* **2025**, *26* (20), No. e202500418.
(6) Shi, D.; Sheng, A.; Chi, L. Glycosaminoglycan-Protein Interactions and Their Roles in Human Disease. *Front. Mol. Biosci.* **2021**, *8*, 639666.
(7) Jin, L.; Abrahams, J. P.; Skinner, R.; Petitou, M.; Pike, R. N.; Carrell, R. W. The anticoagulant activation of antithrombin by heparin. *Proc. Natl. Acad. Sci. U. S. A.* **1997**, *94* (26), 14683−14688.
(8) Möller, S.; Theiß, J.; Deinert, T. I. L.; Golat, K.; Heinze, J.; Niemeyer, D.; Wyrwa, R.; Schnabelrauch, M.; Bogner, E. High-Sulfated Glycosaminoglycans Prevent Coronavirus Replication. *Viruses* **2022**, *14* (2), 413.
(9) Iannuzzi, C.; Irace, G.; Sirangelo, I. The effect of glycosaminoglycans (GAGs) on amyloid aggregation and toxicity. *Molecules* **2015**, *20* (2), 2510−2528.
(10) Vilasi, S.; Sarcina, R.; Maritato, R.; De Simone, A.; Irace, G.; Sirangelo, I. Heparin Induces Harmless Fibril Formation in Amyloidogenic W7FW14F Apomyoglobin and Amyloid Aggregation in Wild-Type Protein In Vitro. *PLoS One.* **2011**, *6* (7), No. e22076.
(11) Solomon, J. P.; Bourgault, S.; Powers, E. T.; Kelly, J. W. Heparin binds 8 kDa gelsolin cross-$\beta$-sheet oligomers and accelerates amyloidogenesis by hastening fibril extension. *Biochemistry* **2011**, *50* (13), 2486−2498.
(12) Ahanger, I. A.; Parray, Z. A.; Nasreen, K.; Ahmad, F.; Hassan, M. I.; Islam, A.; Sharma, A. Heparin Accelerates the Protein Aggregation via the Downhill Polymerization Mechanism: Multi-Spectroscopic Studies to Delineate the Implications on Proteinopathies. *ACS Omega* **2021**, *6* (3), 2328−2339.
(13) Motamedi-Shad, N.; Monsellier, E.; Chiti, F. Amyloid Formation by the Model Protein Muscle Acylphosphatase is Accelerated by Heparin and Heparan Sulphate Through a Scaffolding-based Mechanism. *J. Biochem.* **2009**, *146* (6), 805−814.
(14) Pejler, G.; Sadler, J. E. Mechanism by Which Heparin Proteoglycan Modulates Mast Cell Chymase Activity. *Biochemistry* **1999**, *38* (37), 12187−12195.
(15) Oschatz, C.; Maas, C.; Lecher, B.; Jansen, T.; Björkqvist, J.; Tradler, T.; Sedlmeier, R.; Burfeind, P.; Cichon, S.; Hammerschmidt, S.; et al. Mast Cells Increase Vascular Permeability by Heparin-Initiated Bradykinin Formation In Vivo. *Immunity* **2011**, *34* (2), 258−268.
(16) Cohen, E.; Atzmon, R.; Vlodavsky, I.; Ilan, N. Heparanase processing by lysosomal/endosomal protein preparation. *FEBS Lett.* **2005**, *579* (11), 2334−2338.
(17) Vahdatahar, E.; Daviaud, C.; Main, H.; Havret, R.; Debarnot, C.; Favot-Laforge, L.; Jégou, J. F.; Fruitier-Arnaudin, I.; Dufour, A.; Vivès, R.; et al. The Pathophysiological Functions of Heparanases: From Evolution, Structural and Tissue-Specific Perspectives. *Faseb J.* **2025**, *39* (17), No. e70976.
(18) Tao, Y.; Sun, Y.; Lv, S.; Xia, W.; Zhao, K.; Xu, Q.; Zhao, Q.; He, L.; Le, W.; Wang, Y.; et al. Heparin induces $\alpha$-synuclein to form new fibril polymorphs with attenuated neuropathology. *Nat. Commun.* **2022**, *13* (1), 4226.
(19) Cohlberg, J. A.; Li, J.; Uversky, V. N.; Fink, A. L. Heparin and Other Glycosaminoglycans Stimulate the Formation of Amyloid Fibrils from $\alpha$-Synuclein in Vitro. *Biochemistry* **2002**, *41* (5), 1502−1511.
(20) Snow, A. D.; Mar, H.; Nochlin, D.; Kimata, K.; Kato, M.; Suzuki, S.; Hassell, J.; Wight, T. N. The presence of heparan sulfate proteoglycans in the neuritic plaques and congophilic angiopathy in Alzheimer's disease. *Am. J. Pathol.* **1988**, *133* (3), 456−463.
(21) Stewart, K. L.; Radford, S. E. Amyloid plaques beyond A$\beta$: a survey of the diverse modulators of amyloid aggregation. *Biophy.Rev.* **2017**, *9* (4), 405−419.
(22) Hampel, H.; Hardy, J.; Blennow, K.; Chen, C.; Perry, G.; Kim, S. H.; Villemagne, V. L.; Aisen, P.; Vendruscolo, M.; Iwatsubo, T.; et al. The Amyloid-$\beta$ Pathway in Alzheimer's Disease. *Mol. Psychiatry.* **2021**, *26* (10), 5481−5503.
(23) Chow, V. W.; Mattson, M. P.; Wong, P. C.; Gleichmann, M. An Overview of APP Processing Enzymes and Products. *NeuroMol. Med.* **2010**, *12* (1), 1−12.
(24) Goodger, Z. V.; Rajendran, L.; Trutzel, A.; Kohli, B. M.; Nitsch, R. M.; Konietzko, U. Nuclear signaling by the APP intracellular domain occurs predominantly through the amyloidogenic processing pathway. *J. Cell Sci.* **2009**, *122* (20), 3703−3714.
(25) Huse, J. T.; Liu, K.; Pijak, D. S.; Carlin, D.; Lee, V. M. Y.; Doms, R. W. $\beta$-Secretase Processing in the Trans-Golgi Network Preferentially Generates Truncated Amyloid Species That Accumulate in Alzheimer's Disease Brain. *J. Biol. Chem.* **2002**, *277* (18), 16278−16284.
(26) Pauwels, K.; Williams, T. L.; Morris, K. L.; Jonckheere, W.; Vandersteen, A.; Kelly, G.; Schymkowitz, J.; Rousseau, F.; Pastore, A.; Serpell, L. C.; et al. Structural basis for increased toxicity of pathological a$\beta$42: a$\beta$40 ratios in Alzheimer disease. *J. Biol. Chem.* **2012**, *287* (8), 5650−5660.
(27) Meisl, G.; Yang, X.; Frohm, B.; Knowles, T. P. J.; Linse, S. Quantitative analysis of intrinsic and extrinsic factors in the aggregation mechanism of Alzheimer-associated A$\beta$-peptide. *Sci. Rep.* **2016**, *6* (1), 18728.
(28) Wang, H.; Wu, J.; Sternke-Hoffmann, R.; Zheng, W.; Mörman, C.; Luo, J. Multivariate effects of pH, salt, and Zn2+ ions on A$\beta$40 fibrillation. *Commun. Chem.* **2022**, *5* (1), 171.
(29) Williams, T. L.; Serpell, L. C. Membrane and surface interactions of Alzheimer's A$\beta$ peptide − insights into the mechanism of cytotoxicity. *Febs J.* **2011**, *278* (20), 3905−3917.
(30) Österlund, N.; Kulkarni, Y. S.; Misiaszek, A. D.; Wallin, C.; Krüger, D. M.; Liao, Q.; Mashayekhy Rad, F.; Jarvet, J.; Strodel, B.; Wärmländer, S. K. T. S.; et al. Amyloid-$\beta$ Peptide Interactions with Amphiphilic Surfactants: Electrostatic and Hydrophobic Effects. *ACS Chem. Neurosci.* **2018**, *9* (7), 1680−1692.
(31) Österlund, N.; Lundqvist, M.; Ilag, L. L.; Gräslund, A.; Emanuelsson, C. Amyloid-$\beta$ oligomers are captured by the DNAJB6 chaperone: Direct detection of interactions that can prevent primary nucleation. *J. Biol. Chem.* **2020**, *295* (24), 8135−8144.
(32) Wesén, E.; Gallud, A.; Paul, A.; Lindberg, D. J.; Malmberg, P.; Esbjörner, E. K. Cell surface proteoglycan-mediated uptake and accumulation of the Alzheimer's disease peptide A$\beta$(1−42). *Biochim. Biophys. Acta.* **2018**, *1860* (11), 2204−2214.
(33) Nazere, K.; Takahashi, T.; Hara, N.; Muguruma, K.; Nakamori, M.; Yamazaki, Y.; Morino, H.; Maruyama, H. Amyloid Beta Is Internalized via Macropinocytosis, an HSPG- and Lipid Raft-Dependent and Rac1-Mediated Process. *Front. Mol. Neurosci.* **2022**, *15*, 804702.
(34) Kanekiyo, T.; Zhang, J.; Liu, Q.; Liu, C.-C.; Zhang, L.; Bu, G. Heparan Sulphate Proteoglycan and the Low-Density Lipoprotein Receptor-Related Protein 1 Constitute Major Pathways for Neuronal Amyloid-$\beta$ Uptake. *J. Neurosci.* **2011**, *31* (5), 1644−1651.
(35) Stopschinski, B. E.; Holmes, B. B.; Miller, G. M.; Manon, V. A.; Vaquer-Alicea, J.; Prueitt, W. L.; Hsieh-Wilson, L. C.; Diamond, M. I. Specific glycosaminoglycan chain length and sulfation patterns are required for cell uptake of tau versus $\alpha$-synuclein and $\beta$-amyloid aggregates. *J. Biol. Chem.* **2018**, *293* (27), 10826−10840.
(36) Mandarini, E.; Tollapi, E.; Zanchi, M.; Depau, L.; Pini, A.; Brunetti, J.; Bracci, L.; Falciani, C. Endocytosis and Trafficking of Heparan Sulfate Proteoglycans in Triple-Negative Breast Cancer Cells Unraveled with a Polycationic Peptide. *Int. J. Mol. Sci.* **2020**, *21* (21), 8282.
(37) Berdiaki, A.; Konstantaraki, M.; Ajlan, Z.; Marmara, M.; Tsatsakis, A.; Tzanakakis, G.; Nikitovic, D. Proteoglycans as Regulators of Receptor Trafficking and Spatial Signaling in Cancer. *Cancers* **2026**, *18* (17), 2832.
(38) Payne, C. K.; Jones, S. A.; Chen, C.; Zhuang, X. Internalization and Trafficking of Cell Surface Proteoglycans and Proteoglycan-Binding Ligands. *Traffic* **2007**, *8* (4), 389−401.
(39) Mihov, D.; Raja, E.; Spiess, M. Chondroitin Sulfate Accelerates Trans-Golgi-to-Surface Transport of Proteoglycan Amyloid Precursor Protein. *Traffic* **2015**, *16* (8), 853−870.

Downloaded from pubs.acs.org/jacsat/article-pdf/148/45/49109/6909223/jacs.6c12804.pdf by FORSCHUNGZENTRUM JUELICH user on 26 November 2026

(40) Cataldo, A. M.; Petanceska, S.; Terio, N. B.; Peterhoff, C. M.; Durham, R.; Mercken, M.; Mehta, P. D.; Buxbaum, J.; Haroutunian, V.; Nixon, R. A. Abeta localization in abnormal endosomes: association with earliest Abeta elevations in AD and Down syndrome. *Neurobiol. Aging.* **2004**, *25* (10), 1263−1272.
(41) Pasternak, S. H.; Callahan, J. W.; Mahuran, D. J. The role of the endosomal/lysosomal system in amyloid-beta production and the pathophysiology of Alzheimer's disease: reexamining the spatial paradox from a lysosomal perspective. *J. Alzheimers Dis.* **2003**, *6* (1), 53−65.
(42) Schützmann, M. P.; Hasecke, F.; Bachmann, S.; Zielinski, M.; Hänsch, S.; Schröder, G. F.; Zempel, H.; Hoyer, W. Endo-lysosomal Aβ concentration and pH trigger formation of Aβ oligomers that potently induce Tau missorting. *Nat. Commun.* **2021**, *12* (1), 4634.
(43) Umeda, T.; Tomiyama, T.; Sakama, N.; Tanaka, S.; Lambert, M. P.; Klein, W. L.; Mori, H. Intraneuronal amyloid β oligomers cause cell death via endoplasmic reticulum stress, endosomal/lysosomal leakage, and mitochondrial dysfunction in vivo. *J. Neurosci. Res.* **2011**, *89* (7), 1031−1042.
(44) Marshall, K. E.; Vadukul, D. M.; Staras, K.; Serpell, L. C. Misfolded amyloid-β-42 impairs the endosomal−lysosomal pathway. *Cell. Mol. Life Sci.* **2020**, *77* (23), 5031−5043.
(45) Fromm, J. R.; Hileman, R. E.; Caldwell, E. E. O.; Weiler, J. M.; Linhardt, R. J. Pattern and Spacing of Basic Amino Acids in Heparin Binding Sites. *Arch. Biochem. Biophys.* **1997**, *343* (1), 92−100.
(46) Fukuda, T.; Matsumoto, E.; Miura, Y. Interaction between Multimeric Sulfated Saccharides and Alzheimer Amyloid β (1−42). *Chem. Lett.* **2015**, *44* (11), 1482−1484.
(47) Castillo, G. M.; Lukito, W.; Wight, T. N.; Snow, A. D. The Sulfate Moieties of Glycosaminoglycans Are Critical for the Enhancement of β-Amyloid Protein Fibril Formation. *J. Neurochem.* **1999**, *72* (4), 1681−1687.
(48) Zhou, X.; Wang, Y.; Zheng, W.; Deng, G.; Wang, F.; Jin, L. Characterizing Heparin Tetrasaccharides Binding to Amyloid-Beta Peptide. *Front Mol Biosci.* **2022**, *9*, 824146.
(49) Schäffler, M.; Samantray, S.; Strodel, B. Transition Networks Unveil Disorder-to-Order Transformations in Aβ Caused by Glycosaminoglycans or Lipids. *Int. J. Mol. Sci.* **2023**, *24* (14), 11238.
(50) Miyata, S.; Komatsu, Y.; Yoshimura, Y.; Taya, C.; Kitagawa, H. Persistent cortical plasticity by upregulation of chondroitin 6-sulfation. *Nat. Neurosci.* **2012**, *15* (3), 414−422.
(51) Hirano, K.; Egawa, H.; Nishihara, S. The sulfation pattern of glycosaminoglycans in human brain development and neurological disorders such as Alzheimer's disease. *Am. J. Physiol.: cell Physiol.* **2025**, *329* (3), 801−811.
(52) Ozsan McMillan, I.; Li, J. P.; Wang, L. Heparan sulfate proteoglycan in Alzheimer's disease: aberrant expression and functions in molecular pathways related to amyloid-β metabolism. *Am. J. Physiol.* **2023**, *324* (4), 893−909.
(53) Stewart, K. L.; Hughes, E.; Yates, E. A.; Middleton, D. A.; Radford, S. E. Molecular Origins of the Compatibility between Glycosaminoglycans and Aβ40 Amyloid Fibrils. *J. Mol. Biol.* **2017**, *429* (16), 2449−2462.
(54) Stewart, K. L.; Hughes, E.; Yates, E. A.; Akien, G. R.; Huang, T. Y.; Lima, M. A.; Rudd, T. R.; Guerrini, M.; Hung, S. C.; Radford, S. E.; et al. Atomic Details of the Interactions of Glycosaminoglycans with Amyloid-β Fibrils. *J. Am. Chem. Soc* **2016**, *138* (27), 8328−8331.
(55) Biancalana, M.; Koide, S. Molecular mechanism of Thioflavin-T binding to amyloid fibrils. *Biochim. Biophys. Acta.* **2010**, *1804* (7), 1405−1412.
(56) Tian, Y.; Viles, J. H. pH Dependence of Amyloid-β Fibril Assembly Kinetics: Unravelling the Microscopic Molecular Processes. *Angew. Chem., Int. Ed.* **2022**, *61* (48), No. e202210675.
(57) Yoshimura, Y.; Lin, Y.; Yagi, H.; Lee, Y.-H.; Kitayama, H.; Sakurai, K.; So, M.; Ogi, H.; Naiki, H.; Goto, Y. Distinguishing crystal-like amyloid fibrils and glass-like amorphous aggregates from their kinetics of formation. *Proc. Natl. Acad. Sci. U. S. A.* **2012**, *109* (36), 14446−14451.
(58) Ma, K.; Clancy, E. L.; Zhang, Y.; Ray, D. G.; Wollenberg, K.; Zagorski, M. G. Residue-Specific pKa Measurements of the β-Peptide and Mechanism of pH-Induced Amyloid Formation. *J. Am. Chem. Soc.* **1999**, *121* (38), 8698−8706.
(59) Williamson, M. P. Using chemical shift perturbation to characterise ligand binding. *Prog. Nucl. Magn. Reson. Spectrosc.* **2013**, *73*, 1−16.
(60) Khaled, M.; Rönnbäck, I.; Ilag, L. L.; Gräslund, A.; Strodel, B.; Österlund, N. A Hairpin Motif in the Amyloid-β Peptide Is Important for Formation of Disease-Related Oligomers. *J. Am. Chem. Soc.* **2023**, *145* (33), 18340−18354.
(61) Wälti, M. A.; Orts, J.; Vögeli, B.; Campioni, S.; Riek, R. Solution NMR Studies of Recombinant Aβ(1−42): From the Presence of a Micellar Entity to Residual β-Sheet Structure in the Soluble Species. *ChemBiochem* **2015**, *16* (4), 659−669.
(62) Samantray, S.; Strodel, B. The Effects of Different Glycosaminoglycans on the Structure and Aggregation of the Amyloid-β (16−22) Peptide. *J. Phys. Chem. B.* **2021**, *125* (21), 5511−5525.
(63) Cohen, S. I.; Vendruscolo, M.; Welland, M. E.; Dobson, C. M.; Terentjev, E. M.; Knowles, T. P. Nucleated polymerization with secondary pathways. I. Time evolution of the principal moments. *J. Chem. Phys.* **2011**, *135* (6), 065105.
(64) Cohen, S. I.; Vendruscolo, M.; Dobson, C. M.; Knowles, T. P. Nucleated polymerization with secondary pathways. II. Determination of self-consistent solutions to growth processes described by non-linear master equations. *J. Chem. Phys.* **2011**, *135* (6), 065106.
(65) Cohen, S. I.; Linse, S.; Luheshi, L. M.; Hellstrand, E.; White, D. A.; Rajah, L.; Otzen, D. E.; Vendruscolo, M.; Dobson, C. M.; Knowles, T. P. Proliferation of amyloid-β42 aggregates occurs through a secondary nucleation mechanism. *Proc. Natl. Acad. Sci. U S A.* **2013**, *110* (24), 9758−9763.
(66) Meisl, G.; Yang, X.; Dobson, C. M.; Linse, S.; Knowles, T. P. J. Modulation of electrostatic interactions to reveal a reaction network unifying the aggregation behaviour of the Aβ42 peptide and its variants. *Chem. Sci.* **2017**, *8* (6), 4352−4362.
(67) Beeg, M.; Stravalaci, M.; Romeo, M.; Carrá, A. D.; Cagnotto, A.; Rossi, A.; Diomede, L.; Salmona, M.; Gobbi, M. Clusterin Binds to Aβ1−42 Oligomers with High Affinity and Interferes with Peptide Aggregation by Inhibiting Primary and Secondary Nucleation. *J. Biol. Chem.* **2016**, *291* (13), 6958−6966.
(68) Cohen, S. I.; Vendruscolo, M.; Dobson, C. M.; Knowles, T. P. From macroscopic measurements to microscopic mechanisms of protein aggregation. *J. Mol. Biol.* **2012**, *421* (2−3), 160−171.
(69) Wang, Z.; Patel, V. N.; Song, X.; Xu, Y.; Kaminski, A. M.; Doan, V. U.; Su, G.; Liao, Y.; Mah, D.; Zhang, F.; et al. Increased 3-O-sulfated heparan sulfate in Alzheimer's disease brain is associated with genetic risk gene HS3ST1. *Sci. Adv.* **2023**, *9* (21), No. eadf6232.
(70) Liu, C. C.; Zhao, N.; Yamaguchi, Y.; Cirrito, J. R.; Kanekiyo, T.; Holtzman, D. M.; Bu, G. Neuronal heparan sulfates promote amyloid pathology by modulating brain amyloid-β clearance and aggregation in Alzheimer's disease. *Sci. Transl. Med.* **2016**, *8* (332), 332ra344.
(71) Maninger, J.-K.; Nowak, K.; Goberdhan, S.; O'donoghue, R.; Connor-Robson, N. Cell type-specific functions of Alzheimer's disease endocytic risk genes. *Philos Trans R Soc Lond B Biol Sci.* **2024**, *379*, 1899.
(72) Decker, Y.; Németh, E.; Schomburg, R.; Chemla, A.; Fülöp, L.; Menger, M. D.; Liu, Y.; Fassbender, K. Decreased pH in the aging brain and Alzheimer's disease. *Neurobiol. Aging.* **2021**, *101*, 40−49.
(73) Nohesara, S.; Abdolmaleky, H. M.; Thiagalingam, S. Potential for New Therapeutic Approaches by Targeting Lactate and pH Mediated Epigenetic Dysregulation in Major Mental Diseases. *Biomedicines* **2024**, *12* (2), 457.
(74) Wang, X.; Shao, X.; Yu, L.; Sun, J.; Yin, X.-S.; Chen, Z.; Xu, Y.; Wang, N.; Zhang, D.; Qiu, W.; et al. Changes in the pH value of the human brain in Alzheimer's disease pathology correlated with CD68-positive microglia: a community-based autopsy study in Beijing, China. *Mol. Brain.* **2025**, *18* (1), 10.

Downloaded from pubs.acs.org/jacsat/article-pdf/148/45/49109/6909223/jacs.6c12804.pdf by FORSCHUNGZENTRUM JUELICH user on 26 November 2026


https://doi.org/10.1021/jacs.6c12804
J. Am. Chem. Soc. 2026, 148, 49109−49120

(75) Lepiarz-Raba, I.; Gbadamosi, I.; Florea, R.; Paolicelli, R. C.; Jawaid, A. Metabolic regulation of microglial phagocytosis: Implications for Alzheimer's disease therapeutics. *Transl. Neurodegener* **2023**, *12* (1), 48.
(76) Quick, J. D.; Silva, C.; Wong, J. H.; Lim, K. L.; Reynolds, R.; Barron, A. M.; Zeng, J.; Lo, C. H. Lysosomal acidification dysfunction in microglia: an emerging pathogenic mechanism of neuroinflammation and neurodegeneration. *J. Neuroinflammation* **2023**, *20* (1), 185.
(77) Lindberg, M.; Hu, J.; Sparr, E.; Linse, S. Reduced protein solubility − cause or consequence in amyloid disease? *QRB Discovery* **2025**, *6*, No. e8.
(78) Palmer, A. G. III.NMR Characterization of the Dynamics of Biomacromolecules. *Chem. Rev.* **2004**, *104* (8), 3623−3640.
(79) Khorramian, B. A.; Stivala, S. S. Small-angle x-ray scattering of high- and low-affinity heparin. *Arch. Biochem. Biophys.* **1986**, *247* (2), 384−392.
(80) Edrey, Y. H.; Medina, D. X.; Gaczynska, M.; Osmulski, P. A.; Oddo, S.; Caccamo, A.; Buffenstein, R. Amyloid beta and the longest-lived rodent: the naked mole-rat as a model for natural protection from Alzheimer's disease. *Neurobiol. Aging.* **2013**, *34* (10), 2352−2360.
(81) Buffenstein, R. Negligible senescence in the longest living rodent, the naked mole-rat: insights from a successfully aging species. *J. Comp. Physiol., B.* **2008**, *178* (4), 439−445.
(82) Danielsson, J.; Pierattelli, R.; Banci, L.; Gräslund, A. High-resolution NMR studies of the zinc-binding site of the Alzheimer's amyloid $\beta$-peptide. *Febs J.* **2007**, *274* (1), 46−59.
(83) Syme, C. D.; Nadal, R. C.; Rigby, S. E. J.; Viles, J. H. Copper Binding to the Amyloid-$\beta$ (A$\beta$) Peptide Associated with Alzheimer's Disease. *J. Biol. Chem.* **2004**, *279* (18), 18169−18177.

Downloaded from pubs.acs.org/jacsat/article-pdf/148/45/49109/6909223/jacs.6c12804.pdf by FORSCHUNGZENTRUM JUELICH user on 26 November 2026


https://doi.org/10.1021/jacs.6c12804
*J. Am. Chem. Soc.* 2026, 148, 49109−49120